THE JOURNAL OF PHYSICAL CHEMISTRY B

Article

pubs.acs.org/JPCB

Modeling of Various Optical Spectra in the Presence of Slow Excitation Energy Transfer in Dimers and Trimers with Weak Interpigment Coupling: FMO as an Example

Nicoleta Herascu,[†,#] Adam Kell,[‡,#] Khem Acharya,[‡] Ryszard Jankowiak,[*,‡,§] Robert E. Blankenship,[∥,⊥] and Valter Zazubovich[*,†]

[†]Department of Physics, Concordia University, Montreal, H4B 1R6 Quebec, Canada

[‡]Department of Chemistry and [§]Department of Physics, Kansas State University, Manhattan, Kansas 66506, United States

[∥]Department of Chemistry and [⊥]Department of Biology, Washington University in St. Louis, St. Louis, Missouri 63130, United States

Supporting Information

ABSTRACT: We present an improved simulation methodology to describe nonphotochemical hole-burned (NPHB) spectra. The model, which includes both frequency-dependent excitation energy transfer (EET) rate distributions and burning following EET, provides reasonable fits of various optical spectra including resonant and nonresonant holes in the case of FMO complex. A qualitative description of the NPHB process in light of a very complex protein energy landscape is briefly discussed. As an example, we show that both resonant and nonresonant HB spectra obtained for the 825 nm band of the trimeric FMO of *C. tepidum* are consistent with the presence of a relatively slow EET between the lowest energy states of the monomers of the trimer (mostly localized on BChl *a* 3), with a weak (~1 cm^{-1}) coupling between these states revealed via calculated emission spectra. We argue that the nature of the so-called 825 nm absorption band of the FMO trimer, contrary to the presently accepted consensus, cannot be explained by a single transition.

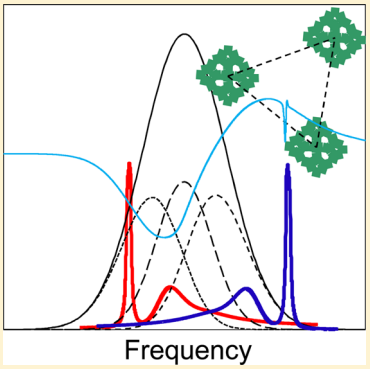

1. INTRODUCTION

Recently we introduced a model describing spectral hole burning (SHB) into two quasi-degenerate bands belonging to pigments connected by relatively slow EET[1] (slow enough to obey Förster theory[2,3]). Although the first version of the model did not include spectral overlaps, it has been successful in qualitatively explaining the shapes of various nonresonant HB spectra and the zero-phonon hole (ZPH) action spectrum in the CP43 antenna complex of Photosystem II (PSII), as well as its fluorescence spectrum. Later the model was extended to the CP43′ ring of the PSI−CP43′ supercomplex, with each A- or B-type pigment having five potential energy acceptors (B or A pigments of the same subunit plus A and B pigments of the adjacent subunits), still with no treatment of spectral overlaps.[4] Simultaneously, proper spectral overlaps have been introduced into the CP43 model, and it has been demonstrated that inclusion of the distribution of the energy transfer rates into the SHB models allows one, for example, to confirm or reject pigment-to-band assignments.[5] In this work we introduce several important refinements/corrections of the model mentioned above, including the process of HB following EET. The model was extended to describe HB spectra (with EET present) in a simple trimer case; to demonstrate its applicability we also model the HB spectra obtained for the FMO complex.[6,7]

Various characteristics of the Fenna−Matthews−Olson (FMO) complex are not fully understood; such as (i) the nature of the lowest energy band, the so-called 825 nm absorption band; (ii) the presence or absence of intermonomer excitation energy transfer (EET); and (iii) the exact origins of various hole burned (HB), fluorescence line narrowed (FLN) and ΔFLN spectra. Even if the trimeric nature of FMO, and the resulting intermonomer EET, are considered important enough to include in model calculations in an attempt to explain its spectroscopic properties, different groups treat the lowest energy 825 nm band as a sum of three bands with either different or identical parameters.[8−11] Competing evidence in favor of different interpretations is available, while spectral holes are notoriously difficult to fit using any of the available models.

2. EXPERIMENTAL SECTION

Absorption spectra of FMO from *Chlorobaculum* (*C.*) *tepidum* have been measured using a Bruker HR125 FTIR spectrometer at 1 cm^{-1} resolution. HB spectra are defined as the difference between postburn and preburn absorption spectra. Emission spectra have been measured using a Princeton Instruments (PI) Acton SP-2300 spectrograph and a PI Acton Spec-10 spectroscopic back-illuminated CCD camera (1340 × 400 pixels). Reported emission spectra were corrected for wave-

Received: October 25, 2013
Revised: February 6, 2014
Published: February 7, 2014

   dx.doi.org/10.1021/jp410586f | *J. Phys. Chem. B* 2014, 118, 2032−2040

length dependence of CCD sensitivity. Care has been taken to analyze spectra measured on the same day. Simulated spectra have been calculated on a laptop PC with Intel Core i7 quad-core processor and 8 GB of RAM. The resolution of calculated spectra was 0.0075 cm^{-1}.

3. RESULTS AND DISCUSSION

It is well accepted in the literature that in the FMO complex bacteriochlorophyll *a* (BChl *a*) 3 (see Figure 1) mostly

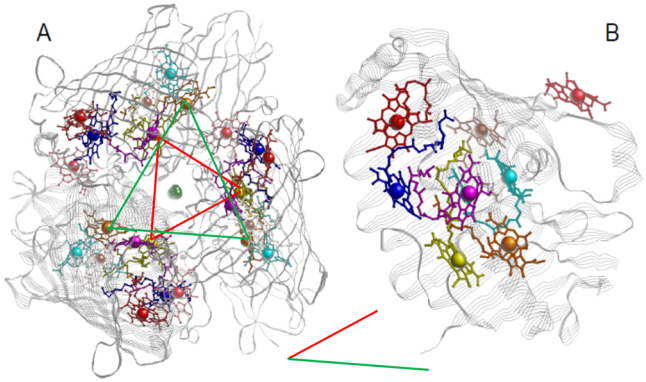

Figure 1. (A) Trimeric structure of the FMO complex, view from the baseplate toward the RC. Red, BChl 1; blue, BChl 2; yellow, BChl 3; orange, BChl 4; cyan, BChl 5; brown, BChl 6; magenta, BChl 7; dark pink, Bchl 8. (B) Side view of one monomer, with bottom toward the RC. The coordinates are taken from the 2.2 Å resolution crystal structure (PDB ID: 3ENI)[12] and drawn with the RasMol program.[13] According to[14,15] the FMO complexes are oriented with BChl 3 and 4 toward the RC. Red and green bars indicate center to center distances between Bchls 3 and 4, respectively, of adjacent monomers.

contributes to the lowest excitonic state in each monomer,[16−18] i.e., to the 825 nm band. Therefore, in our modeling studies (vide infra) of FMO, we first assume that the 825 nm band can be treated as belonging to three BChls 3 (one from each monomer of the FMO trimer) each possessing an identical site-distribution function (SDF).

3.1. Absorption, Emission, and HB Spectra. Figure 2 shows the absorption (solid black) and emission (solid blue) spectra of the *C. tepidum* FMO complex at 5 K. The black

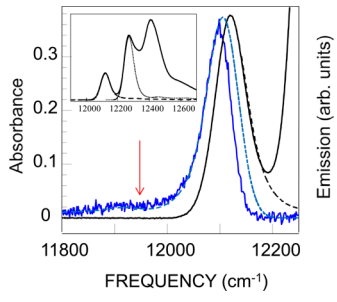

Figure 2. Black solid curve: experimental 5 K absorption spectrum of the *C. tepidum* FMO complex. Dashed black curve: fit to the 825 nm band absorption (see text). Blue solid curve: emission spectrum measured for the same sample as absorption. Dashed blue curve: emission spectrum predicted assuming that emission origin coincides with the full 825 nm band SDF (i.e., there is no intraband/intermonomer EET). The insert shows the entire Q_y absorption band, as well as calculated absorption spectra of 825 nm band and the next absorption band. Arrow indicates 837 nm, see text.

dashed curve shows the fit to the 825 nm band of the FMO absorption spectrum assuming that the 825 nm band can be attributed to three identical pigments (BChl 3) or excitonic states mostly localized on BChl 3, each possessing an identical SDF. In principle, one could produce the same absorption spectrum using three nonidentical SDFs for monomers of the trimer, as long as the sum of these SDFs has the same shape as in the monomer/identical trimer cases, i.e., a Gaussian peaked at 12 116 cm^{-1} with a width of 65 cm^{-1}. The calculated absorption spectrum of the 825 nm band contains contributions from delocalized phonons as well as local BChl *a* vibrations, see the weak tailing to the blue of the 825 nm band in the insert of Figure 2, dashed curve. All relevant parameters are presented in Table 1; thus, reorganization energy is ∼15 cm^{-1}. Also included in the insert is the shifted and renormalized copy of the calculated 825 nm absorption band (dotted curve), simulating absorption of the higher-energy states, which shows a negligible overlap with the 825 nm band. Thus it is clear that second- and third-lowest absorption bands do not significantly contribute to absorption at wavelengths longer than 821 nm, and do not affect the measured width of the 825 nm band, see below. Our experimental emission spectrum does not contain discernible contribution at ∼837 nm (arrow), present in selectively and nonselectively excited emission spectra of ref 11. Thus, we believe the latter might be due to contamination. The blue dashed curve is the emission spectrum obtained by dressing the above Gaussian SDF with the same phonons and local vibrations as used in the fit of the absorption spectrum, see Table 1. The electron−phonon (el-ph) coupling parameters in Table 1 are based on the fit of ΔFLN spectra from[11] (we did not attempt to take into account the 837 nm contribution of ref 11). Note that the calculated emission spectrum is too broad and blue-shifted, compared to the experimental one.

Table 1. SDF and el-ph Coupling Parameters for *C. tepidum* FMO[a]

SDF peak/fwhm	*S*	lognormal PSB[20]: σ/ω_c	peak of PSB
12116 ± 1/65 ± 1 cm^{-1}	0.3	0.7/38 cm^{-1}	23 cm^{-1}

[a]Local BChl *a* vibrations are according to ref 19, with *S*-factors scaled by a factor of 0.7 for better agreement with ΔFLN results of ref 11; a 70 cm^{-1} mode with $S = 0.05$ was also added to the set.

Figure 3A presents the HB spectra obtained for λ_B of 821.0, 823.0, 825.0, 826.5, and 828.4 nm with 120 J/cm^2. The inverted total SDF (see above) is presented for comparison as a light blue curve. It is immediately apparent that the hole depths follow the shape of the SDF. This might be interpreted as indication that intermonomer EET is absent in this system. However, definite conclusions are difficult to make based on resonant depths alone due to the presence of strong NPHB antihole features. In pigment−protein complexes, where NPHB rates are subject to distribution,[21−23] NPHB antiholes must be composed of pigments burning faster than average. Note (vide infra) that even in the absence of EET the resonant ZPH of the calculated hole spectrum for $\lambda_B = 821$ nm is not deep enough. The hypothesis about the absence of EET also is inconsistent with the whole shapes of spectral holes. Additionally, a quick look at emission spectra in Figure 2 indicates that such a conclusion would be premature; namely, the emission spectrum predicted within the no-EET model (dashed blue curve) is too blue-shifted and, more importantly, too broad compared to the experimental emission spectra. While the positions of the bands

dx.doi.org/10.1021/jp410586f | J. Phys. Chem. B 2014, 118, 2032−2040

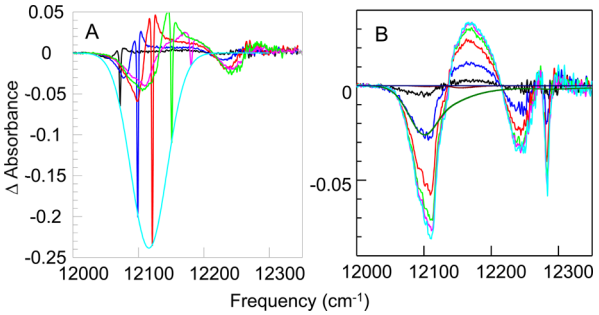

Figure 3. (A) Holes burned at 821.0 (magenta), 823.0 (green), 825.0 (red), 826.5 (dark blue), and 828.4 (black) nm with a fluence of about 120 J/cm^2. Light-blue curve is the inverted full SDF of the 825 nm band. (B) Nonresonant holes produced by illumination at 814 nm with varying fluence. Smooth dark green curve represents the theoretical nonresonant hole in the presence of EET and the absence of an antihole.

could be adjusted by changing the el-ph coupling and phonon sideband parameters, the mirror image law (applied to the 825 nm band alone) dictates that in the absence of intraband EET the width of the emission spectrum must be approximately equal to the width of the absorption spectrum, and this is not the case. The width of the absorption band is ∼72 cm^{-1}, while the width of the emission band is only ∼60 cm^{-1}. We stress that the widths compared here belong to the experimental spectra, and therefore are independent of any simulation parameters. ΔFLN spectra of ref 11 exhibited apparent dependence of phonon-sideband magnitude on excitation wavelength, which most likely indicates the presence of EET. Also note that the absorption spectrum, as well as the HB and emission spectra reported here, were measured on the same day and therefore the discrepancies cannot be attributed to differences in sample preparation and/or reabsorption effects. By analogy with the CP43[1,5] and CP43′[4] antenna complexes, one could suggest that intraband EET is actually present and that emission occurs (mostly) from the lowest energy pigment of the trimer.

Returning to Figure 3A, one should also note a satellite hole at 12 243 cm^{-1} (816.8 nm), which is located to the blue of all the burn wavelengths and therefore must be due to excitonic effects (in the first approximation, be the higher excitonic component of the 825 nm state). Neither the lowest energy nor 816.8 nm holes are conservative, with blue-shifted antiholes exhibiting smaller integral intensity than the hole itself. This suggests coexistence of at least two SHB mechanisms. Regular nonphotochemical HB (NPHB) is responsible for small (on average) blue-shifts, resulting in antiholes in the vicinity of λ_B, as well as for somewhat larger, ∼60 cm^{-1} blue NPHB shifts. These antiholes can easily be seen next to the resonant holes obtained at the longest burn wavelengths (blue and black curves in Figure 3A). As described in refs 24 and 25, the blue NPHB shift of the lowest-energy pigment in an excitonically coupled system must result in a blue shift of the higher exciton states (e.g., 816.8 nm band). However, there must be an additional mechanism that removes pigments from the 825 nm band region; though the nature of this mechanism remains unclear. Thus it is feasible that the lowest energy BChls experience either reversible photochemical burning of unknown nature or NPHB with a drastic blue-shift, resulting in the removal of their absorption far away from the original SDF. We hasten to add that the HB spectra integrated over the whole Q_y region are still nonconservative, although heating the sample up to 120 K perfectly restores the low-temperature absorption spectrum and completely eliminates any holes. One plausible scenario for the reversible photochemical HB mechanism involves electron exchanges (i.e., electron transfer) between BChl 3 and nearby aromatic residues, most likely Phe257, Phe303, and Phe306, by analogy with.[26−28]

Figure 3B contains holes obtained with varying fluence and λ_B of 814 nm, outside of the 825 nm band SDF. Intramonomer EET results in a low-energy hole peaked at 12 105 cm^{-1} (826.1 nm, somewhat fluence-dependent), accompanied by a higher-energy hole at 12 243 cm^{-1} (816.8 nm). Just like the spectra in Figure 3A, these HB spectra are clearly nonconservative. The energy splitting between the two broad holes is about 135 cm^{-1}, and the integral intensity of the holes is approximately twice the integral intensity of the positive feature located between the holes. It is clear that the HB spectra are nonconservative and therefore any NPHB-based model, however well-developed, will not be sufficient to perfectly fit all the HB spectra shown in Figure 3. Nevertheless, in the following we test our improved model of HB in the presence of slow EET[9] to provide more insight into whether or not intermonomer EET takes place and, if present, to estimate the intermonomer couplings from the calculated emission spectra.

3.2. Pigments with Quasidegenerate SDFs Connected by EET. First, we remind the reader of the basic principles of burning into the spectrum of a system where pigments with identical or partially overlapping SDFs are connected by a relatively slow EET.[1,5] Figure 4A resembles that from ref 1 and

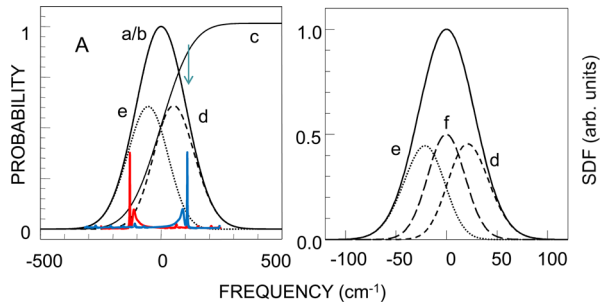

Figure 4. (A) Total SDF and sub-SDFs in the case of two pigments with identical SDFs with fwhm of 250 cm^{-1}. Red curve is the absorption spectrum of a molecule with ZPL relatively low in energy, which is excited at higher energy (blue arrow) via its PSB or vibronic replicas or via EET from higher-energy molecule (blue). (B) The full SDF of three identical pigments with FMO 825 nm band parameters and three sub-SDFs corresponding to the lowest energy pigments (e), pigments with one donor and one acceptor (f) and the highest energy, two-acceptor pigments (d). Zero corresponds to 12 116 cm^{-1} (see text and Table 1 for details).

considers a hypothetical case of two pigments possessing identical SDFs connected by EET. The FMO trimer will represent another example where we assume that three pigments (i.e., one BChl 3 in each monomer of the trimer) or somewhat delocalized states with identical SDFs are connected via slow EET. Returning to the hypothetical dimer, in a given complex one or another pigment can be lower in energy and their energies are independent. Solid overlapping curves a and b (labeled as a/b) shown in Figure 4A represent identical SDFs of pigments 1 and 2, respectively. Curve c reflects the probability that the energy of chromophore 1 (or 2) is lower than the energy on the horizontal axis.

dx.doi.org/10.1021/jp410586f | J. Phys. Chem. B 2014, 118, 2032−2040

Essentially, curve c represents a properly normalized integral of curve a/b. The SDF of a subensemble of pigments 2 (or 1) capable of downhill EET to pigments 1 (or 2) (curve d) is the product of the curves a/b and c, representing the probability of finding pigment 2 (1) at given energy and the probability of finding pigment 1 (2) at an energy lower than the given energy. Curve e, the SDF of a subensemble of pigments being the lowest energy pigments in their complexes, is the difference of curves a/b and d. Summarizing, curve d reflects the sub-SDF of pigments 1 and 2 capable of downhill EET, and curve e reflects the sub-SDF of the pigments 1 and 2 incapable of EET (since they are the lowest energy sites in a complex). Note that curve d can be further represented as a sum of nonidentical sub-SDFs for all possible individual EET rates, see the Supporting Information (SI).

3.3. Distributions of the EET Rates. Introduction of proper donor−acceptor spectral overlaps allows one to make a transition from the binary situation of,[1] with EET either on or off, to the distributions of the EET rates. The latter can be calculated, in Förster approximation, if interpigment coupling is known (e.g., from structure data), from SDF and el-ph coupling parameters. The procedure was described in detail in ref 5. Briefly, the HB master equation including EET rates was introduced as

$$D(\Omega, t) = 1.5 \int d\omega\, L(\Omega - \omega, \tau_{EET}) G(\omega) \int d\lambda\, f(\lambda) \int d\Gamma\, h(\Gamma, \omega) \int d\alpha\, \sin\alpha \cos^2\alpha e^{-P\sigma\phi(\lambda,\Gamma)L(\omega_B-\omega,\tau_{EET})t\cos^2\alpha} \quad (1)$$

Here $h(\Gamma,\omega)$ is the distribution of homogeneous line widths and all other quantities are the same as in refs 5, 21, and 31 For simplicity, our software operates with distributions of the homogeneous line widths, $\Gamma = (2\pi c\tau_{EET})^{-1} + (2\pi c\tau_{fl})^{-1}$ + constant pure dephasing-limited width (the latter is about 1 GHz in FMO at 5 K[29]) rather than distributions of the lifetimes. The SHB quantum yield is given by

$$\phi(\lambda, \tau_{EET}) = \frac{\Omega_0 \exp(-2\lambda)}{\Omega_0 \exp(-2\lambda) + \tau_{fl}^{-1} + \tau_{EET}^{-1}} \quad (2)$$

It is clear that the presence of intermonomer EET will suppress the HB process for higher-energy pigments within the 825 nm band.

Two different approaches are possible to calculating EET involving delocalized protein phonons. On one hand, one can follow the logic of ref 3 and argue that same phonon modes are coupled to both donor and acceptor molecules. As a result, the phonon part of the overlap dependence on donor ZPL−acceptor ZPL overlap should resemble the single-site spectrum itself, rather than a convolution of the donor and acceptor single-site spectra. On the other hand, evidence has been presented recently that the movements of individual BChl *a* molecules in FMO are mostly uncorrelated.[30] Assuming that this lack of correlation extends also to protein environment of the pigment molecules, one would have to follow ref 5 and consider the convolution of single-site spectra. We explored both possibilities and concluded that for relatively small donor−acceptor gaps (intra 825 nm band EET) the EET rates are on average about 10% larger for convolution case, resulting in insignificant differences in calculated optimal interpigment coupling.

In this work, unlike in ref 5, we expand the model to include the frequency-dependent EET-rate distributions. Suppose, we illuminate the system depicted in Figure 4A at the blue edge of the joint SDF of two identical pigments (a/b), as indicated by the blue vertical arrow. The absorption at this wavelength will be dominated by pigments experiencing downhill EET. The distribution of EET rates at λ_B will determine the evolution of the resonant hole (therefore, our earlier results reported for the CP43 antenna complex,[5] which were limited to resonant hole treatment, are still correct). However, the pseudo phonon sideband (PSB) contribution to the hole spectrum originates from pigments excited via their PSB or vibration sidebands. The absorption spectrum of a molecule contributing to the pseudo-PSB is shown by a red curve. Assuming the HB occurs in a vibrationally relaxed state (otherwise eq 2 would have to be modified), the HB yield distribution for such molecules will be determined by the wavelength of the ZPL (burnt via their PSB), not by λ_B. As the probability of EET decreases toward longer wavelengths, the average HB yield should increase. One can generate multiple sub-SDFs, each one corresponding to just one of all the possible EET rates. The sub-SDF for the zero EET rate would be, in the case of two identical pigments depicted in Figure 4A, just curve e. However, sub-SDFs can also be calculated for all other rates. The sum of all sub-SDFs for nonzero rates will yield curve d. These sub-SDFs are, in general, non-Gaussian. For each fixed-rate sub-SDF, the effect of the EET rate on the HB yield (see eq 2) is also fixed, and independent of wavelength. The set of single EET rate sub-SDF for the dimer is presented in the SI.

3.4. Trimer of Identical Pigments/States. In the case of a trimeric complex (e.g., FMO), one has to consider the case of three, rather than two, identical overlapping bands. For three pigments one can think of one donor and two potential acceptors (EET rates have to be summed), and the distribution of the sum of two independent variables is the convolution of the respective distributions. The resulting distribution should start at twice the minimal rate (most likely still zero) and end at twice the maximal rate for a dimer. The three-pigment analog of Figure 4A is presented in Figure 4B. For the sake of consistency with Figure 4A, the lowest energy sub-SDF is still labeled e and the highest energy sub-SDF is labeled d. The middle sub-SDF, corresponding to the pigments with one donor and one acceptor, is labeled f. Again, curves d and f can be further represented as sums of sub-SDFs, each belonging to all pigments with some particular EET rate. By combining various single-rate sub-SDFs with proper weights determined by the emission probabilities, $P_{em} = \tau_{fl}^{-1}/(\tau_{fl}^{-1} + \tau_{EET}^{-1})$one can obtain the emission origin and, subsequently, convoluting it with the single-site emission − the bulk emission spectrum. According to[7] the fluorescence lifetime for FMO at 77 K is 2 ns. Obviously, the contribution of nonzero EET rate sub-SDFs to the emission origin will strongly depend on the interpigment coupling. This should allow for an estimate of interpigment coupling based on a comparison of calculated emission spectra with the measured emission spectrum.

Figure 5A depicts the shapes of the calculated emission origin spectra obtained for the FMO complex using various values for the interpigment coupling within the 825 nm band. For $V > 3$ cm^{-1} the emission origin band is practically indistinguishable from the zero-EET sub-SDF (blue curve in Figure 5A; curve e in Figure 4B). Thus, the spectra are particularly sensitive to small interpigment couplings. The red curve in Figure 5B represents the emission spectrum calculated for FMO assuming that a slow EET is possible due to interpigment coupling of ∼1 cm^{-1}. The insert focuses on the

dx.doi.org/10.1021/jp410586f | J. Phys. Chem. B 2014, 118, 2032−2040

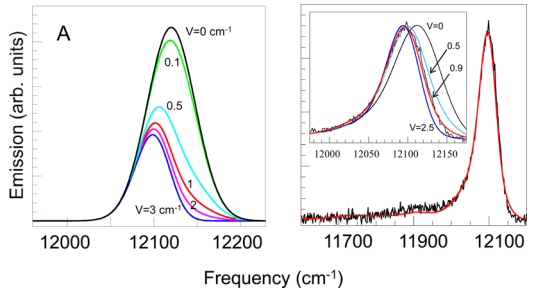

Figure 5. (A) Emission origin bands calculated for the trimeric FMO model with a slow EET. Black curve: total SDF of the 825 nm band; representing the emission origin band when intermonomer coupling is set to zero. Light green curve, $|V| = 0.1$ cm^{-1}; light blue curve, $|V| = 0.5$ cm^{-1}; red curve, $|V| = 1.0$ cm^{-1}; magenta curve, $|V| = 2.0$ cm^{-1}; blue curve, obtained for $|V| = 3.0$ cm^{-1}, is nearly identical to spectrum e from Figure 4B. (B) The red curve (obtained for $|V| = 0.9$ cm^{-1}) represents the best fit to the 5 K measured emission spectrum (black noisy curve). The insert focuses on emission origin region; smooth black, light blue, red, and dark blue curves are emission spectra for $|V| = 0$, 0.5, 0.9, and 2.5 cm^{-1}, respectively.

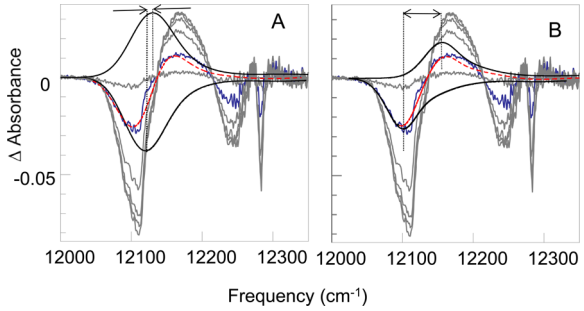

Figure 6. (A) Δ Absorption of nonresonantly burned molecules and antiholes (solid black curves) and their sum (red curve) compared to a representative HB spectrum (blue) in the absence of EET. Nonresonantly burned spectra for other fluences are presented in gray. (B) Similar spectra as frame A but in the presence of EET.

origin region and contains calculated emission spectra for $|V| = 0$, 0.5, 0.9, and 2.5 cm^{-1}. All other parameters are presented in Table 1. As can be seen, although peak position is not very sensitive to coupling for $|V| > 1$ cm^{-1}, the width of the band remains sensitive. It is clear that emission spectrum shape is most sensitive to variations of interpigment coupling below ∼1 cm^{-1}.

3.5. Nonresonant HB Spectra. One could use similar logic and derive, using eq 2, the "origin" of the nonresonantly burned lowest energy hole shown in Figure 3B. In this case, different single-rate sub-SDFs will have to be added with weights proportional to the HB yields given by eq 2. Since the NPHB rate is much smaller than both fluorescence and EET rates, the shape of the "non-resonant hole origin" should be nearly identical to the shape of the emission origin spectrum. The calculated nonresonant hole (dark green) is superimposed with one of the nonresonantly burned holes (blue) in Figure 3B. Note that the dark green curve does not contain any antihole contribution. Fine structure visible in the experimental spectra is most probably due to ZPLs burned through local vibrational modes when exciting at 814 nm. One should note that although the shapes of nonresonant holes apparently support the intermonomer EET hypothesis, one can also explain the nonresonant HB results without invoking intermonomer EET. However, there is a fundamental difference in what one has to do and/or assume in order to simulate the nonresonant holes in the presence and absence of intermonomer EET. In the absence of EET, the lower-energy hole can be produced assuming just a ∼10 cm^{-1} average shift between the original hole (proportional to the whole absorption spectrum) and the antihole; see solid black curves in Figure 6A. In this case, the HB yield does not change with wavelength across the whole 825 nm band. In contrast, in the presence of EET one has to assume an ∼60 cm^{-1} average shift; see Figure 6B. Note that in the latter case, small NPHB shifts are still allowed as long as spectral memory[31] is present, and molecules that experience a small shift can be returned to the original wavelength by subsequent small-shift NPHB following EET from 814 nm pigments to 825 nm pigments. Below, we will use the values of the above shifts as initial guesses for the antihole function in resonant hole fitting. The fractions of absorption "disappearing" in the process of SHB (due to reversible photochemical mechanism suggested above) are 25% in the presence of EET and 9% in the case when EET between monomers is not allowed. These numbers are obtained by comparing the areas of positive (antihole) and negative features (whose difference is the theoretical nonresonant hole, red dashed line) in Figure 6.

3.6. Resonant HB Spectra. Figure 7A presents the 821 nm hole simulated assuming no intermonomer EET. As determined above, in this case the average blue-shift upon burning is 10 cm^{-1}. Obviously, the lowest energy holes are the least affected by potential EET and therefore would look nearly identical regardless of the presence or absence of EET. The highest energy, shortest-λ_B holes (e.g., 821 nm) should be affected by EET the most, if EET is present. The blue curve was produced using the no-memory model described in,[21] while the red curve was produced using the perfect spectral memory model.[31] The burn intensities have been chosen to produce a resonant hole of the same fractional depth as in the experimental spectrum. Note that in the case of perfect spectral memory, where the antihole absorption burns and returns back to the original preburn frequency (except for 10% we allowed to escape far to the blue, see above), the pseudo-PSB part of the hole is strongly suppressed compared to the experiment, while in the case of no-memory the pseudo-PSB is too intense. In

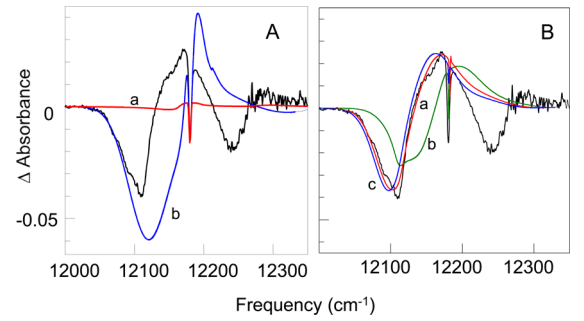

Figure 7. (A) Experimental HB spectrum burned at 821.0 nm (black curve) and calculated HB spectra in the absence of EET and an average blue-shift of the antihole of 10 cm^{-1}. Red curve, a: perfect spectral memory,[31] blue curve, b: no spectral memory.[21] (B) The same experimental hole (black) and the calculated HB spectra for $|V| = 0.9$ cm^{-1} (best fit, red, a); $|V| = 0$ (dark green curve, b) and $|V| = 2.5$ cm^{-1} (blue curve, c) and average NPHB shift of 60 cm^{-1}. The small ∼10 cm^{-1} NPHB shifts are not included, as it was assumed that their net contribution is small when spectral memory in present (see red curve in frame A).

dx.doi.org/10.1021/jp410586f | J. Phys. Chem. B 2014, 118, 2032−2040

both limiting cases, memory-wise, one can see that the broad pseudo-PSB feature is peaked at too high energy if the HB yield is constant across the whole 825 nm band (result of no EET). Thus, in the more realistic case of partial spectral memory (i.e., the case where more than two, but still finite number of spectral positions are available to each pigment molecule) one would expect the pseudo-PSB to be too blue-shifted as well.

Figure 7B presents the simulations of the 821 nm hole assuming the presence of intermonomer EET, with $|V|$ = 0 (blue), 0.9 (red), and 2.5 cm^{-1} (magenta), an average blue-shift of 60 cm^{-1} and no spectral memory. Burning via EET is introduced via corrections to $L(\omega_B-\omega)$ in the exponent of eq 1. The details are presented in the SI section. Qualitatively, allowing for burning via EET results in enhancement of the hole features at energies lower than the laser frequency. One could also note that in the presence of EET, one photon absorbed by the highest energy BChl of the three BChls of a trimer has three chances to cause HB. Overall, it is clear that the calculated red curve in the Figure 7B, though not perfect, provides significantly better fit to experimental data than either curve shown in Figure 7A. Just like in the case of emission spectra, the hole spectra are most sensitive to variations of $|V|$ when $|V| < 1$ cm^{-1}. On the other hand, reasonable fits to the hole spectra could be obtained with couplings up to 2.5 cm^{-1} by varying the parameters of antihole function and λ distribution (not known for FMO; typical values are $\lambda_0 \approx 10$ and $\sigma_\lambda \approx 1.0$[21−23]). The hole spectra are influenced by a larger number of parameters than the emission spectra, and their fits are therefore somewhat less reliable. However, the fits to the hole spectra obtained in the absence of EET are very poor, which allows us to claim that fitting of the hole spectra clearly confirms the presence of EET. Note that one cannot exclude the presence of small, ∼10 cm^{-1} shifts in addition to the ∼60 cm^{-1} shifts in the case of intermonomer EET. These shifts are likely dominant for the lowest energy holes, e.g., for λ_B = 828 nm. For these holes, ∼10 cm^{-1} shifts move the ZPL of a significant fraction of burned molecules to the blue of λ_B, forming the antihole in the immediate vicinity of the resonant hole, while for higher-energy holes, e.g., for λ_B = 821 nm, most molecules remain to the red with respect to λ_B after the 10 cm^{-1} shift. If spectral memory is present, the latter molecules are eventually returned to their preburn condition by subsequent burning. Note how the presence of spectral memory reduces the apparent HB efficiency at longer wavelengths with respect to λ_B in Figure 7A (red curve). Thus, including the 10 cm^{-1} shifts, in addition to the 60 cm^{-1} shifts, would not affect the spectra presented in Figure 7B significantly. On the other hand, an important fault of the spectra simulated in the presence of EET (Figure 7B) is that the resonant HB is reduced at higher energies, in disagreement with the experimental data shown in Figure 1A. First of all, we note that even in the absence of EET the calculated resonant hole at 821 nm is not deep enough. Still, the question arises if there is a meaningful way to explain the deeper experimental holes in the presence of EET?

The model as discussed above does not include excitonic effects, which may affect the shape of the function describing burning via EET (see the SI). Most importantly, as shown in refs 24 and 25 in an excitonically coupled system the shift of the site energy of the lowest energy pigment (due to NPHB) results in a shift of all the exciton states, including the higher ones. We demonstrate it here for a dimer, for the sake of clarity. That is, the transition energies of the two exciton states of a dimer can be expressed as

$$E_{\pm} = (E_H + E_L)/2 \pm \sqrt{V^2 + ((E_H - E_L)/2)^2}$$

where E_H and E_L are site energies (transition energies in the absence of interaction) of higher and lower-energy pigments in the dimer, respectively. If NPHB results in the shift of the site energy E_L by ΔE_L, the energy of the higher exciton state will shift by

$$\Delta E_+ = \frac{\Delta E_L}{2}\left(1 + \frac{(E_L - E_H)}{\sqrt{4V^2 + ((E_H - E_L))^2}}\right)$$

Note that $E_L - E_H < 0$ and the square root is defined as positive.

We assume that additional HB of the higher-energy pigments would be observable when the spectral shift of the higher exciton state is larger than the homogeneous line width. The fraction of systems experiencing an observable excitonic burning effect depends on interpigment coupling V, the SDF parameters and the distribution of shifts (antihole function). If V is small and the donor−acceptor gap is large, the small shift of the lower-energy pigment has almost no effect on the higher energy state. On the other hand, if the antihole function is broad enough (for instance, when pigments are free to shift within the whole SDF and beyond), this "excitonic higher-state burning" may be present in a large fraction of trimers, even for small coupling V. We also need to stress that due to this effect, the higher-energy states will appear to be burning resonantly with the same rate as the lower-energy states, see eq 2 with ${\tau_{EET}}^{-1} = 0$. Interestingly, this would mean that there would be no preference for resonant burning of pigments with the slowest EET or no EET, and the widths of even shallow holes would reflect the average EET rate, not necessarily the slower end of the EET rate distribution. The average EET time calculated for V = 0.9 cm^{-1} for the middle of the 825 nm band is 360 ps, which can be compared to 117 ps reported in ref 29. Achieving agreement with ref 29 requires increasing intermonomer coupling to ∼1.5 cm^{-1}, which results in a somewhat poorer fits to the emission spectra, but still provides a rather good agreement when taking experimental uncertainties into account.

It is not clear if resonant burning attributable to the excitonic effect discussed above was ever observed in any system. The apparent absence of such an effect was considered in[25] as evidence in favor of Redfield EET models. However, it may be quite possible that FMO possesses the necessary combination of small coupling (justifying the use of Förster EET model), small SDF width (ensuring large $E_H - E_L$ are unlikely) and an antihole function with large average spectral shift. Figure 8 depicts distributions of higher-state shifts obtained for the above parameters and $|V|$ = 1.5 cm^{-1} via Monte Carlo simulations. Obviously, a significant fraction of complexes exhibits higher-state shifts exceeding the homogeneous line width, and therefore contribute to this indirect HB of higher excitonic states. Most of the higher state shifts are to the blue, but occasionally, red shifts are possible when the shift of the lowest-energy pigment changes the order of the pigment site energies (e.g., the lowest-energy one becomes the second-lowest, etc). More rigorous modeling of this quasi-resonant excitonic burning effect is beyond the scope of this manuscript and will be a subject of future publications, as it requires

dx.doi.org/10.1021/jp410586f | J. Phys. Chem. B 2014, 118, 2032−2040

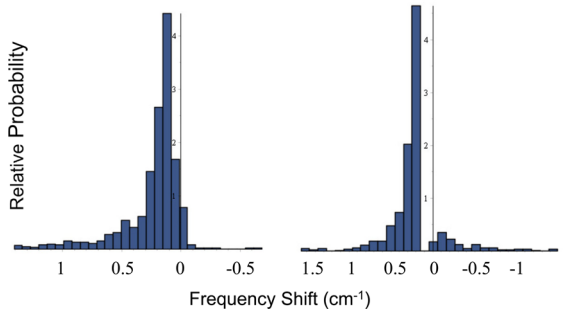

Figure 8. Probability distributions of shifts of the second-lowest (one donor one acceptor, left) and the highest-energy (two acceptors, right) pigments of the trimer with identical FMO-like SDFs upon 60 cm^{-1} blue shift of the lowest-energy pigment. V = 1.5 cm^{-1}. Courtesy of Stephanie Larocque.

combining (i) burning via EET; (ii) the presence of spectral memory (here the approaches similar to those employed in ref 31 could be used to keep track of excitonic interactions in a trimer); and (iii) more than one tier of the protein energy landscape in the same program.

One might observe that an interpigment coupling of ∼1 cm^{-1} is much lower than that predicted for BChl 3 of adjacent monomers by structure-based calculations, see Table 2. Note

Table 2. Couplings between BChls of Adjacent Trimers in cm^{-1} Calculated Using TrEsp Method[32] Assuming an Effective μ^2 = 25.2 D^2[a]

	1A	2A	3A	4A	5A	6A	7A	8A
1C	**1.3**	0.6	−0.6	0.7	2.8	1.5	1.2	21.3
2C	1.9	**-0.3**	−2.9	−2.2	9.2	5.8	2.6	4.2
3C	1.7	0.4	**-2.5**	5.7	5.5	2.4	5.2	0.6
4C	0.4	0.6	0.5	**2.4**	−0.9	−0.4	2.4	−1.3
5C	0.8	1.1	1.4	−0.4	**2.2**	0.0	−0.9	3.3
6C	0.0	0.9	0.8	1.8	−1.9	**-1.7**	2.2	−7.9
7C	0.4	0.4	−0.8	5.8	−2.1	0.3	**7.5**	−9.3
8C	0.0	0.6	0.8	−1.1	1.5	−1.2	−2.8	**4.3**

[a]Couplings between identical BChls are highlighted in bold. V_{33} is −2.5 cm^{-1}.

that the matrix is not symmetric with respect to the diagonal since rows and columns belong to different monomers of the trimer. This may mean either that (i) the dielectric constant of the protein environment between these pigments has not been estimated properly; (ii) the transition dipole of the 825 nm excitonic state has less favorable orientation than that of "pure" BChl 3 due to contributions from other pigments; or, finally, (iii) the widespread assignments of the 825 nm band to BChl 3 are incorrect. The latter possibility is very unlikely, based on many recent theoretical calculations (see ref 18 for review). Thus, we return to the possibility of the transition dipole of the lowest state of the FMO monomer being different with respect to that of "pure" BChl 3. One could employ the extended Förster model as described for example for LH2 in refs 33−35. However, since we are only considering EET between the lowest-energy states of the aggregates (FMO monomers), there may be no need to explore the overlaps between the whole density of states (DOS) including higher excitonic states, as was done in refs 33−35. Excitonic calculations with Hamiltonians available in the literature[16,17,30,36−39] consistently result in the oscillator strength of the lowest state of the FMO monomer being somewhat lower than that of monomeric BChl *a*. A quick look at the Frame A of Figure 1 suggests that the distances between BChls 4 of adjacent FMO monomers are significantly larger than distance between BChls 3. Thus, although it might be difficult to precisely determine the effective location of the transition dipole of the state delocalized between BChls 3 and 4, one can safely argue that the distance between the dipoles of the delocalized lowest states of the monomers is not smaller than that between BChls 3. Finally, we compared the orientation factors entering the expression for coupling between BChls 3 and between the somewhat delocalized lowest states of the FMO monomers. The Hamiltonian from[36] leads to a change of the orientation factor from −0.4 (for BChls 3) to −0.3. Hamiltonians[16,17,38,39] result in reduction of the orientation factor by at least a factor of 10. The Hamiltonian of ref 37 leads to a slight increase of the orientation factor magnitude to −0.45. However, site energies assignments of this Hamiltonian are rather exotic, and the oscillator strength of the 825 nm band is only 0.6 BChl equivalents (per monomer). The Hamiltonian from ref 30 leads to an orientation factor of −0.12. Thus, it appears rather plausible that excitonic effects result in a decrease of effective coupling by a factor of about two.

4. CONCLUDING REMARKS

We successfully demonstrated full inclusion of EET-related effects into a spectral hole burning model, which requires a very small increase in computational complexity and time. The approach relies on introducing (in lieu of frequency-dependent EET rate distributions) nonidentical sub-SDF for each EET rate, as opposed to identical ones of ref 5. It appears that for $|V|$ > 3 cm^{-1} hole spectra and emission spectra are dominated by the lowest-energy trap pigments, while spectra are extremely sensitive to variations in interpigment coupling in $0 < |V| < 1$ cm^{-1} region.

We argue that NPHB results (both resonant and nonresonant spectra) obtained for the 825 nm band in trimeric FMO of *C. tepidum* are consistent with the presence of a relatively slow EET between the lowest energy states of the monomers of the trimer, with a weak (∼1−2 cm^{-1}) coupling between these states revealed via calculated emission and hole spectra. The above model provides reasonable fits of various optical spectra including resonant and nonresonant holes. Further possible improvements of the model were also briefly described; to accomplish these we need to improve our understanding of the protein energy landscape, which determines the distributions of spectral shifts and respective HB yields, as well as the degree of spectral memory involved (research in progress).

It also appears that HB in the FMO complex is due to two processes. The first is NPHB involving small (∼ 10 cm^{-1}) spectral shifts with a high degree of spectral memory. The second process likely involves the next tier of the protein energy landscape, with average (blue) shifts of ∼60 cm^{-1} upon burning. It cannot be excluded that excitonic effects (V_{34}, V_{35}, V_{37}, etc. within a monomer) contribute to the apparent 60 cm^{-1} shifts or that some reversible photochemical process (e.g., electron transfer from BChl to surrounding residues) is involved. The 60 cm^{-1} shift in the absorption of BChl 3 of a single monomer results in noticeable spectral shifts of all states of the trimer due to intermonomer coupling (V_{33}).

dx.doi.org/10.1021/jp410586f | J. Phys. Chem. B 2014, 118, 2032−2040

■ ASSOCIATED CONTENT

Supporting Information

Details of the modeling procedure, examples of nonidentical sub-SDF, and EET probability function. This material is available free of charge via the Internet at http://pubs.acs.org.

■ AUTHOR INFORMATION

Corresponding Authors

*E-mail: ryszard@ksu.edu.

*E-mail: valter.zazubovits@concordia.ca.

Author Contributions

#These authors equally contributed to this work.

Notes

The authors declare no competing financial interest.

■ ACKNOWLEDGMENTS

Research at Concordia has been supported by NSERC Discovery and Concordia University funds. R.J. acknowledges support from the Chemical Sciences, Geosciences and Biosciences Division, Office of Basic Energy Sciences, Office of Science, U.S. Department of Energy (Grant No. DE-FG02-11ER16281). FMO samples were prepared and supplied by Dr. J. Wen during his time at Washington University in St. Louis. The authors are thankful to Dr. Tõnu Reinot (Iowa State University/Ames Laboratory USDOE) for providing the code of the HB program used in ref 31 and fruitful discussions on the HB model with spectral memory. We acknowledge Stephanie Larocque, CEGEP Ahuntsic, for her participation in calculations of higher-state shifts upon HB of the lowest-energy pigment (Figure 8).

■ REFERENCES

(1) Zazubovich, V.; Jankowiak, R. On the Energy Transfer between Quasi-degenerate States with Uncorrelated Site Distribution Functions: An Application to the CP43 Complex of Photosystem II. *J. Lumin.* **2007**, *127*, 245−250.

(2) Förster, T. Zwischenmolekulare Energiewanderung und Fluoreszenz. *Ann. Physik* **1948**, *437*, 55−75.

(3) van Amerongen, H.; Valkunas, L.; van Grondelle, R. *Photosynthetic Excitons*; : Singapore, 2000.

(4) Feng, X.; Neupane, B.; Acharya, K.; Zazubovich, V.; Picorel, R.; Seibert, M.; Jankowiak, R. Spectroscopic Study of the CP43′ Complex and the PSI−CP43′ Supercomplex of the Cyanobacterium *Synechocystis* PCC 6803. *J. Phys. Chem. B* **2011**, *115*, 13339−13349.

(5) Herascu, N.; Ahmouda, S.; Picorel, R.; Seibert, M.; Jankowiak, R.; Zazubovich, V. Effects of the Distributions of Energy or Charge Transfer Rates on Spectral Hole Burning in Pigment−Protein Complexes at Low Temperatures. *J. Phys. Chem. B* **2011**, *115*, 15098−15109.

(6) Wen, J.; Harada, J.; Buyle, K.; Yuan, K.; Tamiaki, H.; Ohoka, H.; Loomis, R. A.; Blankenship, R. E. Characterization of an FMO Variant of *Chlorobaculum tepidum* Carrying Bacteriochlorophyll a Esterified by Geranylgeraniol. *Biochemistry* **2010**, *49*, 5455−5463.

(7) Freiberg, A.; Lin, S.; Timpmann, K.; Blankenship, R. E. Exciton Dynamics in FMO Bacteriochlorophyll-protein at Low Temperatures. *J. Phys. Chem. B* **1997**, *101*, 7211−7220.

(8) Louwe, R. J. W.; Vrieze, J.; Aartsma, T. J.; Hoff, A. J. Toward an Integral Interpretation of the Optical Steady-State Spectra of the FMO-Complex of *Prosthecochloris aestuarii*. 1. An Investigation with Linear-Dichroic Absorbance-Detected Magnetic Resonance. *J. Phys. Chem. B* **1997**, *101*, 11273−11279.

(9) Matsuzaki, S.; Zazubovich, V.; Rätsep, M.; Hayes, J. M.; Small, G. J. Energy Transfer Kinetics and Low Energy Vibrational Structure of the Three Lowest Energy Qy-states of the Fenna-Matthews-Olson Antenna Complex. *J. Phys. Chem. B* **2000**, *104*, 9564−9572.

(10) Hayes, J. M.; Ruehlaender, M.; Soukoulis, C. M.; Small, G. J. Monte Carlo Simulation of Energy Transfer Rates: Application to Downward Energy Transfer within the 825nm Absorption Band of the FMO Complex of *Prosthechochloris aestuarii*. *J. Lumin.* **2002**, *98*, 246−255.

(11) Rätsep, M.; Freiberg, A. Electron−phonon and Vibronic Couplings in the FMO Bacteriochlorophyll *a* Antenna Complex Studied by Difference Fluorescence Line Narrowing. *J. Lumin.* **2007**, *127*, 251−259.

(12) Tronrud, D. E.; Wen, J.; Gay, L.; Blankenship, R. E. The Structural Basis for the Difference in Absorbance Spectra for the FMO Antenna Protein from Various Green Sulfur Bacteria. *Photosynth Res.* **2009**, *100*, 79−87.

(13) Sayle, R. S.; Milner-White, E. J. RASMOL: Biomolecular Graphics for All. *Trends Biochem. Sci.* **1995**, *20*, 374−376.

(14) Wen, J.; Zhang, H.; Gross, M. L.; Blankenship, R. E. Membrane Orientation of the FMO Antenna Protein from *Chlorobaculum tepidum* as Determined by Mass Spectrometry-based Footprinting. *Proc. Natl. Acad. Sci. U.S.A.* **2009**, *106*, 6134−6139.

(15) Huang, R.Y.-C.; Wen, J.; Blankenship, R. E.; Gross, M. L. Hydrogen−Deuterium Exchange Mass Spectrometry Reveals the Interaction of Fenna−Matthews−Olson Protein and Chlorosome CsmA Protein. *Biochemistry* **2012**, *51*, 187−193.

(16) Vulto, S.; De Baat, M.; Louwe, R.; Permentier, H.; Neef, T.; Miller, M.; van Amerongen, H.; Aartsma, T. J. Exciton Simulations of Optical Spectra of the FMO Complex from the Green Sulfur Bacterium *Chlorobium tepidum* at 6 K. *J. Phys. Chem. B* **1998**, *102*, 9577−9582.

(17) Cho, M.; Vaswani, H. M.; Brixner, T.; Stenger, J.; Fleming, G. R. Exciton Analysis in 2D Electronic Spectroscopy. *J. Phys. Chem. B* **2005**, *109*, 10542−10556.

(18) Milder, M. T. W.; Brüggemann, B.; van Grondelle, R.; Herek, J. L. Revisiting the Optical Properties of the FMO Protein. *Photosynth. Res.* **2010**, *104*, 257−274.

(19) Zazubovich, V.; Tibe, I.; Small, G. J. Bacteriochlorophyll *a* Franck−Condon Factors for the $S_0 \rightarrow S_1(Q_y)$ Transition. *J. Phys. Chem. B* **2001**, *105*, 12410−12417.

(20) Kell, A.; Feng, X.; Reppert, M.; Jankowiak, R. On the Shape of the Phonon Spectral Density in Photosynthetic Complexes. *J. Phys. Chem. B* **2013**, *117*, 7317−7323.

(21) Grozdanov, D.; Herascu, N.; Reinot, T.; Jankowiak, R.; Zazubovich, V. Low-Temperature Protein Dynamics of the B800 Molecules in the LH2 Light-Harvesting Complex: Spectral Hole Burning Study and Comparison with Single Photosynthetic Complex Spectroscopy. *J. Phys. Chem. B* **2010**, *114*, 3426−3438.

(22) Herascu, N.; Najafi, M.; Amunts, A.; Pieper, J.; Irrgang, K.-D.; Picorel, R.; Seibert, M.; Zazubovich, V. Parameters of the Protein Energy Landscapes of Several Light-Harvesting Complexes Probed via Spectral Hole Growth Kinetics Measurements. *J. Phys. Chem. B* **2011**, *115*, 2737−2747.

(23) Najafi, M.; Herascu, N.; Seibert, M.; Picorel, R.; Jankowiak, R.; Zazubovich, V. Spectral Hole Burning, Recovery, and Thermocycling in Chlorophyll−Protein Complexes: Distributions of Barriers on the Protein Energy Landscape. *J. Phys. Chem. B* **2012**, *116*, 11780−11790.

(24) Reppert, M.; Zazubovich, V.; Dang, N. C.; Seibert, M.; Jankowiak, R. Low-Energy Chlorophyll States in the CP43 Antenna Protein Complex: Simulation of Various Optical Spectra. II. *J. Phys. Chem. B* **2008**, *112*, 9934−9947.

(25) Reppert, M. Modeling of Resonant Hole-Burning Spectra in Excitonically Coupled Systems: The Effects of Energy-Transfer Broadening. *J. Phys. Chem. Lett.* **2011**, *2*, 2716−2721.

(26) Dashdorj, N.; Zhang, H.; Kim, H.; Yan, J.; Cramer, W. A.; Savikhin, S. The Single Chlorophyll a Molecule in the Cytochrome b_6f Complex: Unusual Optical Properties Protect the Complex against Singlet Oxygen. *Biophys. J.* **2005**, *88*, 4178−4187.

(27) Peterman, E. J.; Wenk, S.-O.; Pullerits, T.; Pålsson, L.-O.; van Grondelle, R.; Dekker, J. P.; Rogner, M.; van Amerongen, H. Fluorescence and Absorption Spectroscopy of the Weakly Fluorescent

Chlorophyll a in Cytochrome b6f of *Synechocystis* PCC6803. *Biophys. J.* **1998**, *75*, 389−398.
(28) Li, Y.-F.; Zhou, W.; Blankenship, R. E.; Allen, J. P. Crystal Structure of the Bacteriochlorophyll a Protein from *Chlorobium tepidum*. *J. Mol. Biol.* **1997**, *271*, 456−471.
(29) Rätsep, M.; Blankenship, R.; Small, G. J. Energy Transfer and Spectral Dynamics of the Three Lowest Energy Q_y-States of the Fenna-Matthews-Olson Antenna Complex. *J. Phys. Chem. B* **1999**, *103*, 5736−5741.
(30) Olbrich, C.; Strümpfer, J.; Schulten, K.; Kleinkathöfer, U. Quest for Spatially Correlated Fluctuations in the FMO Light-Harvesting Complex. *J. Phys. Chem. B* **2011**, *115*, 758−764.
(31) Reinot, T.; Dang, N. C.; Small, G. J. A Model for Persistent Hole Burned Spectra and Hole Growth Kinetics that Includes Photoproduct Absorption: Application to Free Base Phthalocyanine in Hyperquenched Glassy Ortho-dichlorobenzene at 5 K. *J. Chem. Phys.* **2003**, *119*, 10404−10414.
(32) Madjet, M. E.; Abdurahman, A.; Renger, T. Intermolecular Coulomb Couplings from Ab Initio Electrostatic Potentials: Application to Optical Transitions of Strongly Coupled Pigments in Photosynthetic Antennae and Reaction Centers. *J. Phys. Chem. B* **2006**, *110*, 17268−17281.
(33) Scholes, G. D.; Fleming, G. R. On the Mechanism of Light Harvesting in Photosynthetic Purple Bacteria: B800 to B850 Energy Transfer. *J. Phys. Chem. B* **2000**, *104*, 1854−1868.
(34) Jang, S.; Newton, M. D.; Silbey, R. J. Multichromophoric Förster Resonance Energy Transfer. *Phys. Rev. Lett.* **2004**, *92*, 218301.
(35) Sumi, H. Theory on Rates of Excitation-Energy Transfer between Molecular Aggregates through Distributed Transition Dipoles with Application to the Antenna System in Bacterial Photosynthesis. *J. Phys. Chem. B* **1999**, *103*, 252−260.
(36) Hayes, D.; Engel, G. S. Extracting the Excitonic Hamiltonian of the Fenna-Matthews-Olson Complex Using Three-Dimensional Third-Order Electronic Spectroscopy. *Biophys. J.* **2011**, *100*, 2043−2052.
(37) Fidler, A. F.; Caram, J. R.; Hayes, D.; Engel, G. S. Towards a Coherent Picture of Excitonic Coherence in the Fenna−Matthews−Olson Complex. *J. Phys. B* **2012**, *45*, 154013.
(38) Vulto, S. I. E.; de Baat, M. A.; Neerken, S.; Nowak, F. R.; van Amerongen, H.; Amesz, J.; Aartsma, T. J. Excited State Dynamics in FMO Antenna Complexes from Photosynthetic Green Sulfur Bacteria: A Kinetic Model. *J. Phys. Chem. B* **1999**, *103*, 8153−8161.
(39) Adolphs, J.; Renger, T. How Proteins Trigger Excitation Energy Transfer in the FMO Complex of Green Sulfur Bacteria. *Biophys. J.* **2006**, *91*, 2778−2797.